The effects of surface roughness on the transient characteristics of hydrodynamic cylindrical bearings during startup

Shuhui Cui, Le Gu, Michel Fillon, Liqin Wang, Chuanwei Zhang

The effects of surface roughness on the transient characteristics of hydrodynamic cylindrical bearings during startup

Shuhui Cui[a,b], Le Gu[a], Michel Fillon[b], Liqin Wang [a,c], and Chuanwei Zhang [a]*

[a] MIIT Key Laboratory of Aerospace Bearing Technology and Equipment, Harbin Institute of Technology, Harbin 150001, China

[b] Pprime Institut, CNRS-Université de Poitiers-ISAE-ENSMA, Futuroscope Chasseneuil, 86962, France

[c] State Key Laboratory of Robotics and System, Harbin Institute of Technology, Harbin 150080, China

*Corresponding author: zhchwei@hit.edu.cn

Abstract

The effect of surface roughness on the transient characteristics of the hydrodynamic cylindrical bearing during startup is studied. A mixed lubrication model considering both asperity contact and hydrodynamic fluid flow is solved. The asperity contact pressure is obtained by the Greenwood-Williamson (GW) contact model. The hydrodynamic pressure is calculated by modified average Reynolds equation with finite element method (FEM). The transient movement of the journal center, the transient average film thickness, the hydrodynamic pressure and the contact pressure are presented for different surface roughnesses. The contact time and contact zone in different types of surface roughness are obtained. The influences of the standard deviation of asperity height (σ) and rough surface patterns on these parameters are analyzed. The results show that the surface roughness has an important influence on the transient characteristics of the bearing during the initial period of startup.

Keywords: hydrodynamic bearing, mixed lubrication, surface roughness, surface pattern, startup

1 Introduction

For the hydrodynamic bearings without auxiliary support system, the mixed lubrication is critical for frequent startup operation in overload conditions. The minimum film thickness of the bearings during early startup is on the same level as the asperity height of the rough surfaces [1]. Asperity contact of the shaft and bearing surface can be generated [2, 3], leading to serious wear of the bearing surface, power loss, and seizures [4]. Under the mixed lubrication, both the asperity contact pressure and the hydrodynamic pressure are influenced by the asperity height and surface roughness pattern [5]. Therefore, the effects of surface roughness on the startup characteristics of the hydrodynamic cylindrical bearings must be understood.

Christensen et al. [6] numerically presented the effects of surface roughness on the hydrodynamic behavior of the journal bearing. They found that generally the surface roughness had slight impacts on the carrying capacity of journal bearings. However, when the eccentricity ratio closed to the hydrodynamic limit, the structure and statistical properties of surface roughness had a strong impact on the carrying capacity of the bearings. The rough surface in transverse orientation could enhance the carrying capacity, but the one in longitudinal orientation would decrease the carrying capacity.

Patir and Cheng [7, 8] developed an average Reynolds equation considering the effects of the directional patterns of surface roughness. Based on this model, Wang et al. [9-11] built a mixed-THED model to analyze the conformal contact between the rough surfaces for the journal bearings. They concluded that the asperity contact/sliding friction and the viscous friction could be evaluated using the roughness-relate friction correction factor and the shear stress factor of the average Reynolds equation [7, 8]. Sander et al. [12] analyzed the effect of surface roughness on the dynamic properties of the journal bearing running from hydrodynamic lubrication to mixed lubrication. They found that comparing to the rough surface of a new bearing, a run-in rough surface could decrease both maximum contact pressure and contact area. Dobrica et al. [13, 14] proposed a numerical method of

deterministic roughness to research on the hydrodynamic component in mixed lubrication. They found that transverse roughness could increase both minimum film thickness and friction torque, while longitudinal roughness only influenced the friction torque. The isotropic roughness had a little influence on both film thickness and friction torque.

Many works have been done for understanding the startup properties of hydrodynamic journal bearings [15-17]. Mokhtar et al. [18, 19] tested the wear characteristics of journal bearings during repeated startup. They concluded that the discernable wear was entirely generated by the sliding contacts during early startup. The wear localization changes with different surface roughnesses. Bouyer et al. [20] experimentally found that the mixed lubrication of hydrodynamic bearings occurs just in the initial running of the journal during startup. The rougher surfaces could increase the friction coefficient, except for the large isotropic roughness. They maintained that it was essential to consider the roughness of the shaft and bearing surfaces to get accurate result.

Sugimura et al. [21] experimentally investigated the influence of surface roughness pattern on the lubricated running-in process of pure rolling/sliding contact. They found that the longitudinal roughness generated very thin steady films. The surface micro-texture influenced the wear rate of surface in running-in process. Krupka et al. [22] presented that rough surfaces could impact the film forming of hydrodynamic bearings during startup. They found that compared to smooth surfaces, the shallow rough features could be more efficient for the separation of the rubbing surfaces in mixed lubrication. Also, asperity interactions in transient conditions could be lowered by well-designed topography of rough surface. In addition, many works [23-26] were conducted to understand the influences of surface roughness on mixed lubrication regime. However, to the published papers, there are few investigations about the evolution of transient parameters of hydrodynamic cylindrical bearings during startup, such as hydrodynamic pressure and contact pressure.

In this paper, the influence of surface roughness on the transient behavior of the hydrodynamic cylindrical bearing during startup are studied. The evolutions of both asperity contact force and hydrodynamic bearing force during startup are presented. The variations of transient hydrodynamic pressure, transient contact pressure, as well as minimum film thickness in different surface roughnesses during startup are obtained. Also, the impacts of different types of surface roughness on contact time and contact zone are analyzed.

2 Models and formulation

2.1 Geometric modeling

Fig. 1 shows the schematic of a hydrodynamic cylindrical bearing with a fixed bearing surface and a rotating shaft. The bearing starts up under the constant applied load W. At beginning of startup, the asperity contact occurs due to the insufficient hydrodynamic bearing force for supporting the shaft. The initial minimum film thickness h is not zero, which is assumed to be the average gap between the two average surface heights (Fig. 1 (b)). It is determined by the asperity contact force F_c and the applied load W combined with the expression $h=C+e\cos(\theta-\varphi)$.

In our model, the thermal effect is ignored because the startup period is very short. The misalignment in the axial direction is not considered. At the very early initial stage of startup, the friction force drives the shaft to roll along the bush surface in the opposite direction of rotation, then the shaft falls back and forms a very small minimum film thickness. With the increase in the shaft speed, there is a small hydrodynamic pressure, and the influence of the friction force is not so significant. Therefore, we mainly focus on the center locus in the rotating direction after the very beginning period. As a consequence, the friction force between the two contacted surfaces and the hydrodynamic shear stresses which occur on the body surface are neglected.

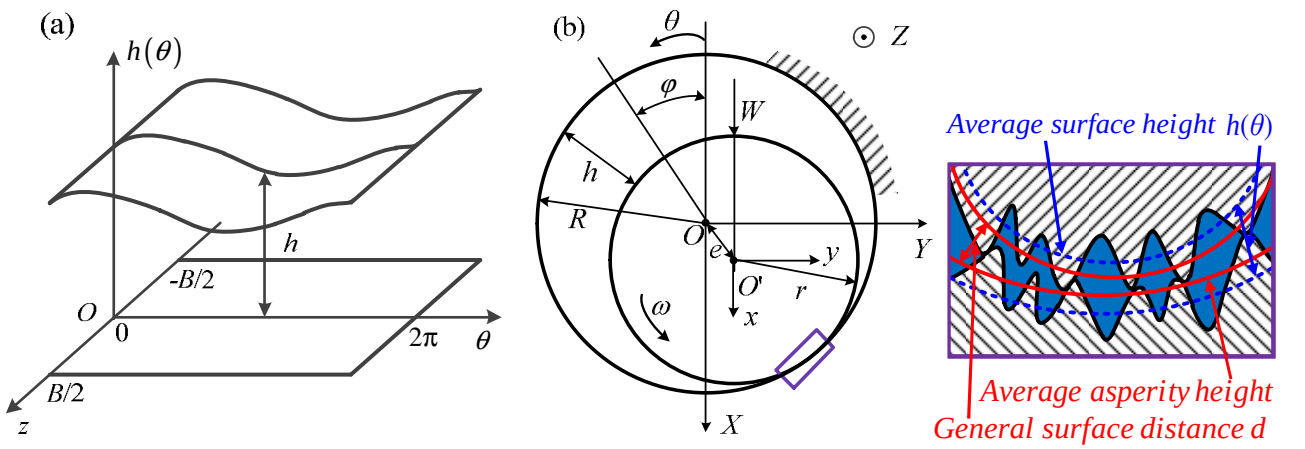

Fig. 1. The coordinate system and characteristics of the hydrodynamic cylindrical bearing during startup, (a) the coordinate system, and (b) the movement and the asperity contact property of the bearing

The fundamental dynamic law applied to the shaft leads two equations in the x and y directions respectively, as follows:

$$m\ddot{x}(t)=F_{cx}(t)+F_{hx}(t)+W \tag{1a}$$

$$m\ddot{y}(t)=F_{cy}(t)+F_{hy}(t) \tag{1b}$$

where F_c and F_h represent the contact force and hydrodynamic bearing force, respectively. The subscripts of x and y represent in x and y directions, respectively, as shown in Fig. 1 (b). m is the mass of the shaft. t is the time.

2.2 Governing equations

In the model, the lubricant is laminar Newtonian fluid and incompressible. The modified average Reynolds equation [27] is used for calculating the hydrodynamic pressure

$$\frac{\partial}{r\partial\theta}\left(\Phi_\theta\frac{h^3}{\mu}\frac{\partial p}{r\partial\theta}\right)+\frac{\partial}{\partial z}\left(\Phi_z\frac{h^3}{\mu}\frac{\partial p}{\partial z}\right)=6u\Phi_c\frac{\partial h}{r\partial\theta}+6u\sigma\frac{\partial\Phi_s}{r\partial\theta}+12\Phi_c\frac{\partial h}{\partial t} \tag{2a}$$

where $\sigma=\sqrt{\sigma_1^2+\sigma_2^2}$ is the standard deviation of asperity height, the subscripts 1 and 2 represent the shaft and bearing surface, respectively. μ is the dynamic viscosity of the lubricant. u is the shaft surface velocity.

Using the following non-dimensional parameters

$$\lambda=\frac{z}{B},\ H=\frac{h}{C},\ \psi=\frac{C}{r},\ \frac{p}{P}=\frac{2\mu\omega}{\psi^2},\ \bar{\sigma}=\frac{\sigma}{C},\ U=\frac{u}{r\omega},\ \tau=\omega t$$

The nondimensional average Reynolds equation can be obtained as

$$\frac{\partial}{\partial\theta}\left(\Phi_\theta H^3\frac{\partial P}{\partial\theta}\right)+\left(\frac{r}{B}\right)^2\frac{\partial}{\partial\lambda}\left(\Phi_z H^3\frac{\partial P}{\partial\lambda}\right)=3U\Phi_c\frac{\partial H}{\partial\theta}+3\bar{\sigma}U\frac{\partial\Phi_s}{\partial\theta}+6\Phi_c\frac{\partial H}{\partial\tau} \tag{2b}$$

The Φ_θ, and Φ_z are the pressure flow factors in circumferential direction and axial direction, respectively, and Φ_s is the shear flow factor [7, 8]. Φ_c is the contact factor [27]. The factors are the function of surface roughness as following

$$\Phi_\theta=\Phi_z(H',1/\gamma)=\begin{cases}1-c'e^{-r'H'},\ \gamma\le 1\\ 1+c'e^{-r'},\ \gamma>1\end{cases} \tag{3a}$$

$$\Phi_s = V_{r1}\phi_s\left(H',\gamma_1\right) - V_{r2}\phi_s\left(H',\gamma_2\right) \tag{3b}$$

$$\Phi_c = \begin{cases} e^{-0.6912+0.782H'-0.304H'^2+0.0401H'^3}, 0 \le H' \le 3 \\ 1 \qquad\qquad\qquad\qquad\qquad\quad , H' > 3 \end{cases} \tag{3c}$$

The parameters of V_{r1}, V_{r2} and ϕ_s are given by

$$V_{r1} = 1 - V_{r2} = \left(\frac{\sigma_1}{\sigma}\right)^2 \tag{3d}$$

$$\phi_s = \begin{cases} A_1 H'^{\alpha_1} e^{-\alpha_2 H' + \alpha_3 H'^2}, H' \le 5 \\ A_2 e^{-0.25H'} \qquad\qquad , H' > 5 \end{cases} \tag{3e}$$

where H' is the Stribeck ratio, $H' = h/\sigma$. γ is the surface pattern parameter. The other coefficients related to the rough surface pattern are listed in Table 1.

Table 1 Coefficients of Φ_x, Φ_y and Φ_s (H'>0.5) [8]

Surface pattern	γ	c'	r'	A_1	A_2	α_1	α_2	α_3
Transverse	1/6	1.38(H'>1)	0.42(H'>1)	1.962	1.754	1.08	0.77	0.03
Isotropic	1	0.90	0.56	1.899	1.126	0.98	0.92	0.05
Longitudinal	6	0.520	1.5	1.290	0.388	0.62	1.09	0.08

For calculating the asperity contact pressure, the Greenwood-Williamson (GW) contact model is applied [28]. The normal contact force per unit area, i.e., the conformal contact pressure $\rho(\theta, z)$ between shaft and the bearing surfaces, is calculated by [29]

$$\rho(\theta,\ z) = D_{sum}\int_d^{+\infty} \overline{P}(\overline{z}-d) f\left(\overline{z}\right) \mathrm{d}\overline{z} \tag{4}$$

where the individual asperity contact force $\overline{P}$ dependents on each asperity's inference $\varpi = \overline{z} - d$, $\overline{P} = \frac{4}{3} E'\sqrt{R_p}(\varpi)^{3/2}$. $\overline{z}$ and d represent the standard separation and the general surface distance between two conformal rough surfaces. $f\left(\overline{z}\right)$ is the density function of Gaussian distribution.

The asperity contact forces in the x and y directions are written as

$$\begin{cases} F_{cx} = r\int_0^{2\pi}\int_0^B \rho(\theta,z)\cos\theta \mathrm{d}z\mathrm{d}\theta \\ F_{cy} = r\int_0^{2\pi}\int_0^B \rho(\theta,z)\sin\theta \mathrm{d}z\mathrm{d}\theta \end{cases} \tag{5}$$

2.3 Solution procedure

Using the Newmark method, the motion equation (Eq.(1)) is expressed by

$$\begin{cases} \dot{x}_{t+\Delta t}(t) = \dot{x}_t + \left[(1-\alpha)\ddot{x}_t + \alpha\ddot{x}_{t+\Delta t}\right]\Delta t \\ x_{t+\Delta t}(t) = x_t + \dot{x}_t\Delta t + \left[\left(\frac{1}{2}-\beta\right)\ddot{x}_t + \beta\ddot{x}_{t+\Delta t}\right]\Delta t^2 \end{cases} \tag{6a}$$

$$\begin{cases} \dot{y}_{t+\Delta t}(t) = \dot{y}_t + \left[(1-\alpha)\ddot{y}_t + \alpha\ddot{y}_{t+\Delta t}\right]\Delta t \\ y_{t+\Delta t}(t) = y_t + \dot{y}_t\Delta t + \left[(\frac{1}{2}-\beta)\ddot{y}_t + \beta\ddot{y}_{t+\Delta t}\right]\Delta t^2 \end{cases} \tag{6b}$$

where $x, \dot{x}, \ddot{x}$ and $y, \dot{y}, \ddot{y}$ are the displacements, velocities and accelerations of the journal center in the x and y directions, respectively. Δt is the time step. The subscripts t and $t+\Delta t$ are the present and next time steps, respectively. The constant coefficients α and β are set to be 0.5 and 0.25, respectively.

The nondimentional Reynolds equation Eq.(2b) is calculated by finite element method. The Reynolds boundary condition is used. The weak elemental formation of Reynolds equation is deduced as

$$\begin{aligned}&-\iint_{\Omega_e}\left\{\Phi_\theta H^3\frac{\partial N}{\partial\theta}\frac{\partial \mathrm{d}P}{\partial\theta}+\Phi_z H^3\left(\frac{r}{B}\right)^2\frac{\partial N}{\partial\lambda}\frac{\partial \mathrm{d}P}{\partial\lambda}\right\}\mathrm{d}\Omega_e\\&=\iint_{\Omega_e}\left\{\Phi_\theta H^3\frac{\partial P_0}{\partial\theta}\frac{\partial N}{\partial\theta}+\Phi_z H^3\left(\frac{r}{B}\right)^2\frac{\partial P_0}{\partial\lambda}\frac{\partial N}{\partial\lambda}+3\Phi_c N\left(U\frac{\partial H}{\partial\theta}+2\frac{\partial H}{\partial\tau}\right)+3\bar{\sigma}UN\frac{\partial\Phi_s}{\partial\theta}\right\}\mathrm{d}\Omega_e\end{aligned}\tag{7a}$$

where the weighting functions N are taken to be the shape functions of triangular element as follows:

$$\begin{cases}N_1(\xi,\eta)=1-\xi-\eta\\N_2(\xi,\eta)=\xi\\N_3(\xi,\eta)=\eta\end{cases}\tag{7b}$$

where ξ and η are the nondimentional coordinates of the elements, $-1\le\xi,\eta\le 1$.

The nondimentional hydrodynamic pressure P and the pressure change δP over each element are interpolated by

$$\begin{cases}P=\sum_{j=1}^{3}N_j(\xi,\eta)P_j\\\delta P=\sum_{j=1}^{3}N_j(\xi,\eta)\delta P_j\end{cases}\tag{7c}$$

where P_j and δP_j are the nondimentional hydrodynamic pressure and pressure change at each node.

The matrix equation for calculating the hydrodynamic pressure over each triangular element is

$$[K_{3\times3}]\{\delta P_{3\times1}\}=R_{3\times1}\tag{7d}$$

where the matrix elements are

$$\begin{cases}K_{ij}=\mathop{\mathrm{I}}_{\text{Gauss}}\left\{\Phi_\theta H^3\frac{\partial N_i}{\partial\theta}\frac{\partial N_j}{\partial\theta}+\Phi_z H^3\left(\frac{r}{B}\right)^2\frac{\partial N_i}{\partial\lambda}\frac{\partial N_j}{\partial\lambda}\right\}\\R_i=-\mathop{\mathrm{I}}_{\text{Gauss}}\left\{\Phi_\theta H^3\frac{\partial P_0}{\partial\theta}\frac{\partial N_i}{\partial\theta}+\Phi_z H^3\left(\frac{r}{B}\right)^2\frac{\partial P_0}{\partial\lambda}\frac{\partial N_i}{\partial\lambda}+3\Phi_c N_i\left(U\frac{\partial H}{\partial\theta}+2\frac{\partial H}{\partial\tau}\right)+3\bar{\sigma}UN_i\frac{\partial\Phi_s}{\partial\theta}\right\}\end{cases}\tag{7e}$$

For calculating the hydrodynamic pressure at each time step, an inner iteration is conducted. For example, in the nth time step, the initial hydrodynamic pressure P_0^n is the one obtained in the last time step P^{n-1}, i.e., $P_0^n=P^{n-1}$. The change in the hydrodynamic pressure δP_k^n at each node is calculated using Eq.(7a-7e). Then the pressure becomes $P_k^n=P_{k-1}^n+\delta P_k^n$. The calculation is repeated until the convergence criterion is met, i.e., $|\delta P_k^n-\delta P_{k-1}^n|<10^{-3}$.

The hydrodynamic bearing forces in the x and y directions are expressed as

$$\begin{cases}F_{hx}=r\int_0^{2\pi}\int_0^B p(\theta,z)\cos\theta\,\mathrm{d}z\,\mathrm{d}\theta\\F_{hy}=r\int_0^{2\pi}\int_0^B p(\theta,z)\sin\theta\,\mathrm{d}z\,\mathrm{d}\theta\end{cases}\tag{8}$$

The general process is as follows:

1. At beginning of t=0, the shaft is static and the rotational speed is zero. The applied load W is completely sustained by the asperity contact force in the x direction. By this, the initial film thickness and contact pressure are determined.

2. With the increasing rotational speed during startup, hydrodynamic pressure and hydrodynamic bearing force are obtained by calculating average Reynolds equation Eq.(2) and Eq.(8). Meanwhile, the contact pressure and the asperity contact force are obtained by calculating the contact model (Eq.(4) and Eq.(5)).

3. The displacements, velocities and accelerations of the journal center at each time step are calculated using the motion equations (Eq.(1) and Eq.(6)). The corresponding average film thickness is obtained.

4. The hydrodynamic bearing force, asperity contact force and the motion properties are calculated iteratively until the end of the acceleration of the bearing during startup.

3 Results and Discussion

3.1 Verification

The results of present numerical model are compared to the experimental results presented by Mokhtar et al. [17, 19] in Fig. 2. Mokhtar's experimental parameters are listed in Table 2. The rotational speed is set to rise up to 850 rpm within 0.3 second. The simulation results of both the contact time (Fig. 2 (a)) and the journal center trajectories (Fig. 2 (b)) are in accordance with that in the experiments.

Table 2 Parameters for Mokhtar's tests

Parameters	**Values**
Bearing diameter (mm)	74.653
Bearing length (mm)	76.20
Diametral clearance (mm)	0.121
Equivalent modulus (GPa)	210
Poisson's ratio	0.29
Surface roughness of the shaft (μm)	0.12
Surface roughness of the bearing (μm)	1.473
Oil viscosity (Pa·s)	0.074

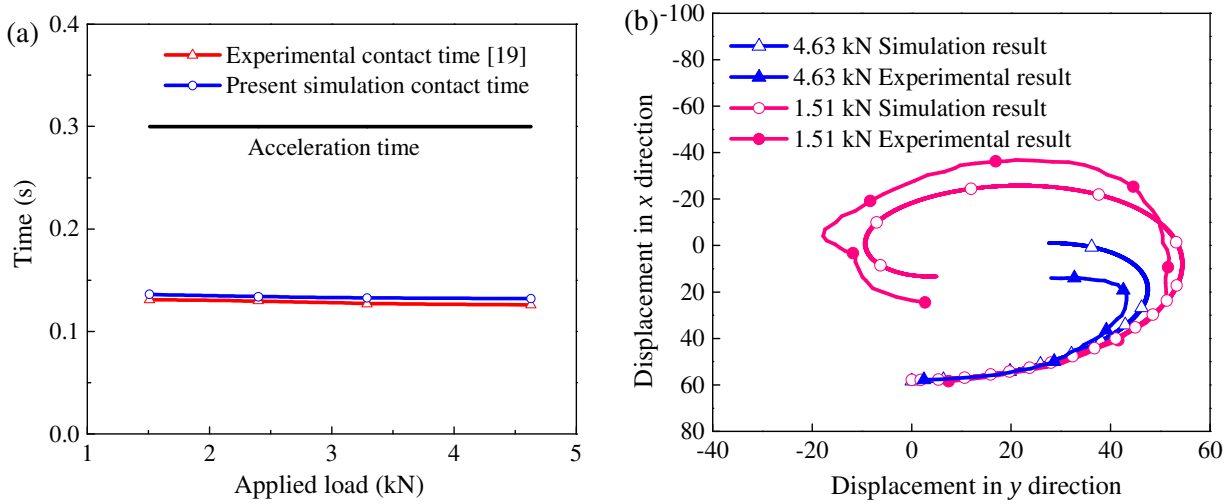

Fig. 2 Comparison between Mokhtar's experimental results and the present simulation results, (a) the contact time in the acceleration time of 0.3 s, and (b) the journal center trajectory within 0.3 s under the applied loads of 1.51 kN and 4.63 kN, respectively.

3.2 Startup operation

During startup, the rotational speed rises linearly up to 1000 rpm within 0.1 s. The standard deviation of asperity height σ is 1 μm. The surface roughness direction is in isotropic orientation. The simulation parameters are listed in Table 3.

Table 3 The simulation conditions

Parameters	**Symbols**	**Values**
Bearing radius (mm)	R_b	50.1
Bearing length (mm)	B	60
Shaft radius (mm)	r	50
Relative radius clearance	ψ	2‰
Areal asperity density (asp/m^2)	D_{sum}	5e11
Asperity radius (μm)	R_p	2
Equivalent modulus (GPa)	$E_{1,2}$	210
Poisson's ratio	$\nu_{1,2}$	0.29
Oil density of ISO T32 (kg/m^3)	ρ	860
Oil viscosity of ISO T32 at 20°C (Pa·s)	μ	0.027
Mass of the rotor (kg)	m	400
Applied load (kN)	W	4

Fig. 3 shows the variations of hydrodynamic bearing force and asperity contact force in startup operation. The resultant hydrodynamic force and resultant contact force are assumed to be $F_h = \sqrt{F_{hx}^2 + F_{hy}^2}$ and $F_c = \sqrt{F_{cx}^2 + F_{cy}^2}$ respectively, while the negative of the scale represents the inverse direction of the coordinate system (Fig. 1 (b)). We observe that the shaft lifts off at the time t=0.057 s, when the lift-off speed is ω=570 rpm. This period of the mixed lubrication before the shaft separates with the bearing surface is named the contact time [19]. During the contact time, the resultant hydrodynamic bearing force and resultant contact force in the x direction are larger than that in the y direction. This is because that the applied load is in the x direction. The composition of contact force and hydrodynamic force are mainly used to support the applied load.

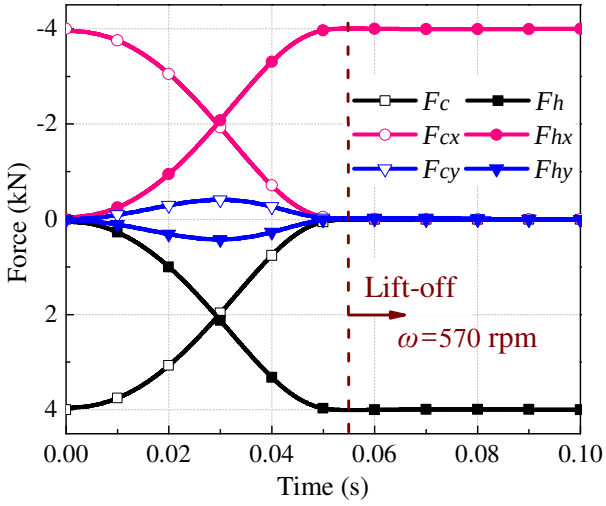

Fig. 3 The variations of hydrodynamic bearing force and asperity contact force of the hydrodynamic cylindrical bearing in startup operation

Fig. 4 shows the transient behavior of hydrodynamic cylindrical bearing during startup. In initial period of startup, the shaft mainly slides along the bearing surface with a quickly increasing attitude angle θ and a slightly increasing eccentricity ratio ε. The attitude angle θ=38 degree during the contact time t_c=0.057 s is named as asperity contact zone (Fig. 4 (a)). During startup of the bearing, the minimum film thickness keeps increasing,

while the transient hydrodynamic (HD) pressure first increases and then decreases (Fig. 4 (b)). The maximum HD pressure appears at the time t_{pmax}=0.047 s (Fig. 4 (b)) before the shaft separates with the bearing surface at the time t_c=0.057 s (Fig. 4 (a)). This is due to the effect of both the film thickness and the increasing rotational speed. From the very beginning of startup until the time t_{pmax}=0.047 s, the minimum film thickness keeps almost constant (Fig. 4 (b)). The slowly rotating shaft squeezes the lubricant oil into the small clearance between the two surfaces, causing an increase in the HD pressure. Then, after t_{pmax}=0.047 s, the minimum film thickness increases quickly, and this squeeze effect decreases, leading to a decrease in the HD pressure. In addition, the active zone of HD pressure keeps increasing (Fig. 4 (c)), while the contact zone keeps being about 20 degree (Fig. 4 (d)).

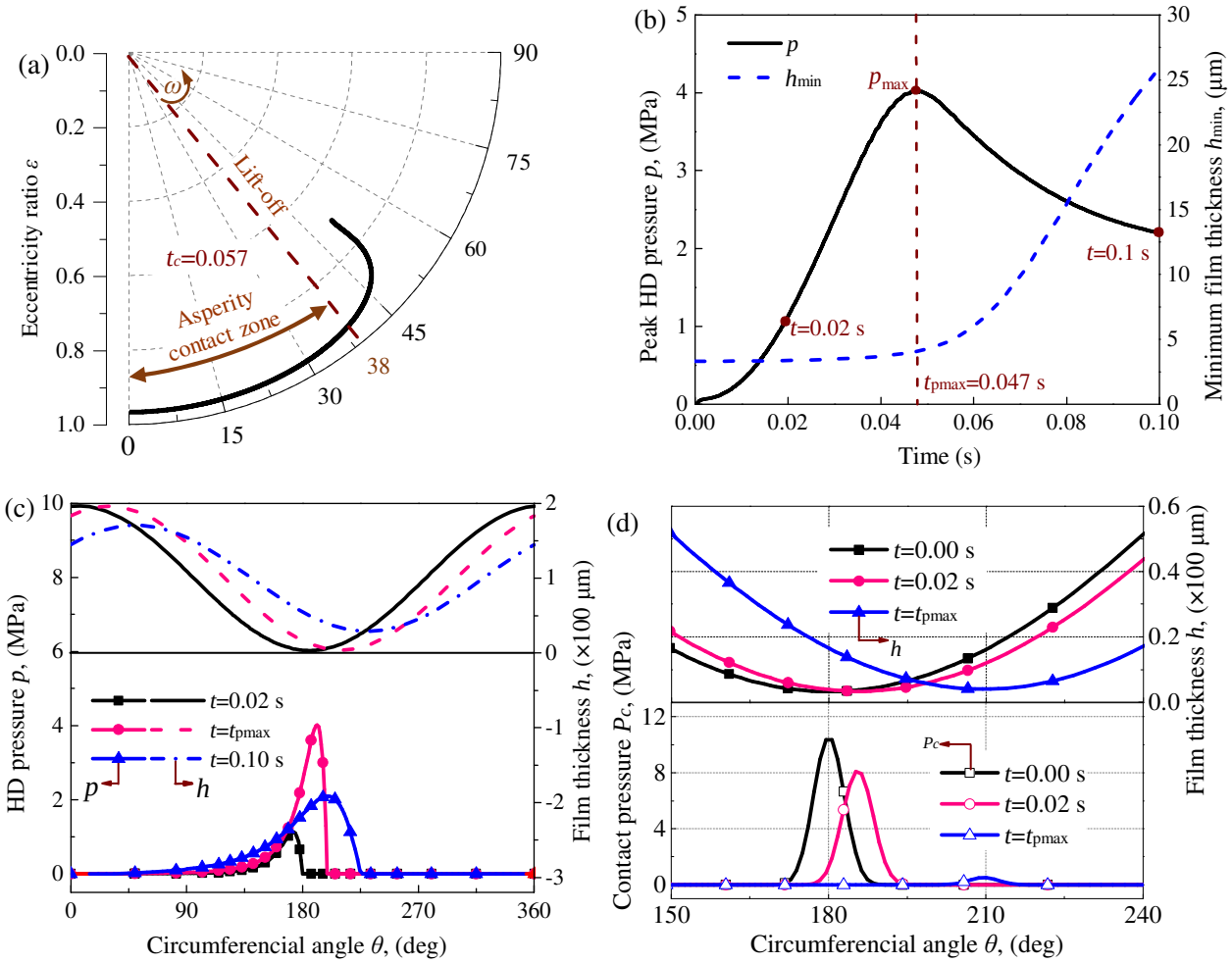

Fig. 4 The transient movement and pressure properties of hydrodynamic cylindrical bearing during startup, (a) journal center locus in clearance circle, (b) the variation of peak hydrodynamic (HD) pressure and average minimum film thickness, (c) the distribution of HD pressure, and (d) the distribution of contact pressure in the plane of z=0 at different times

3.3 Effect of standard deviation of asperity height σ

Fig. 5 shows the hydrodynamic bearing force and asperity contact force changing with standard deviation of surface roughness σ during startup. The rotational speed rises linearly up to 1000 rpm within 0.1 second. The surface roughness is in isotropic orientation. σ is set to be 1.00 μm, 0.75 μm and 0.50 μm, respectively. It is observed that a high σ leads to a low hydrodynamic bearing force, resulting in a large contact force, a long contact time, and a high lift-off speed (Fig. 5 (a)). However, in the y direction, an increasing σ can increase both asperity contact force and hydrodynamic bearing force (Fig. 5 (b)). The asperity contact force has a reverse direction with

the hydrodynamic bearing force.

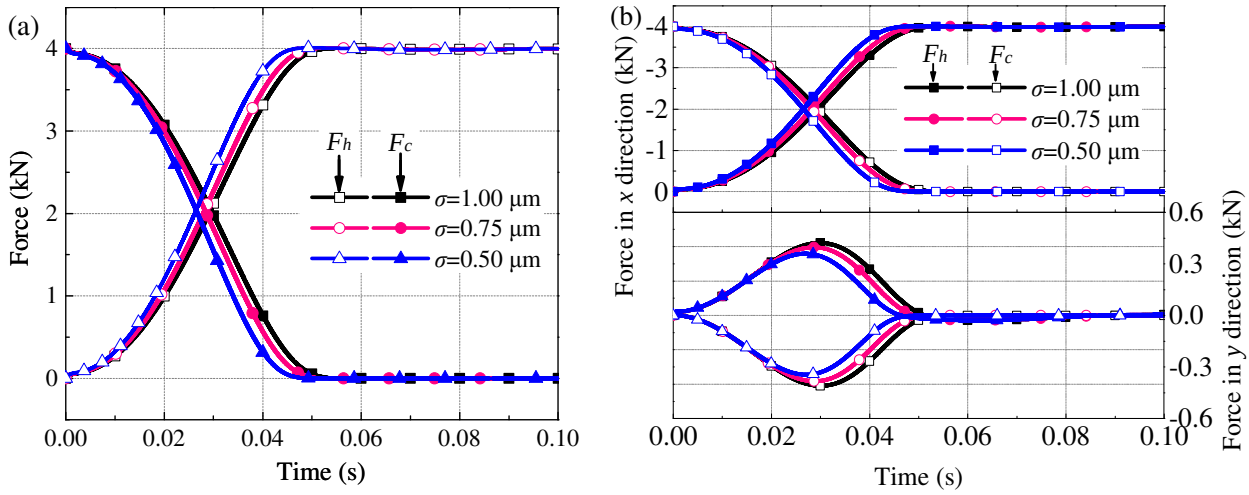

Fig. 5 The variations of hydrodynamic bearing force F_h and asperity contact force F_c of the hydrodynamic cylindrical bearing in different standard deviation of asperity heights σ during startup, (a) the resultant forces, (b) component forces of F_h and F_c in the x and y directions

Fig. 6 describes the transient characteristics of the hydrodynamic cylindrical bearing variates with the standard deviation of asperity height σ during startup. We observe that a small σ leads to a large eccentricity ratio but a small contact zone (Fig. 6 (a) and (b)). The minimum film thickness decreases with an increasing eccentricity ratio (Fig. 6 (b)), leading to an increasing hydrodynamic pressure (Fig. 6 (c)). Interestingly, in the mixed lubrication during contact time, the Stribeck ratio h_{min}/σ as a function of σ is almost the same (Fig. 6 (d)), while the hydrodynamic pressure is significantly influenced by σ (Fig. 6 (c)). However, in the hydrodynamic lubrication when the shaft is lifted up, the Stribeck ratio h_{min}/σ decreases rapidly with an increase in σ (Fig. 6 (d)), while the hydrodynamic pressure changes slowly (Fig. 6 (c)). This is because that in mixed lubrication, σ has a significant effect on the contact factor Φ_c (Eq.(2)). A large σ represents a high contact possibility for a single asperity, which generates a larger average film thickness between two rough surfaces.

In addition, as shown in Fig. 6 (c), for σ=0.5, 0.75 and 1 μm, the peak HD pressure first increases and then decreases, reaching the maximum at the time t_{pmax}=0.041, 0.046 and 0.049 s, respectively.

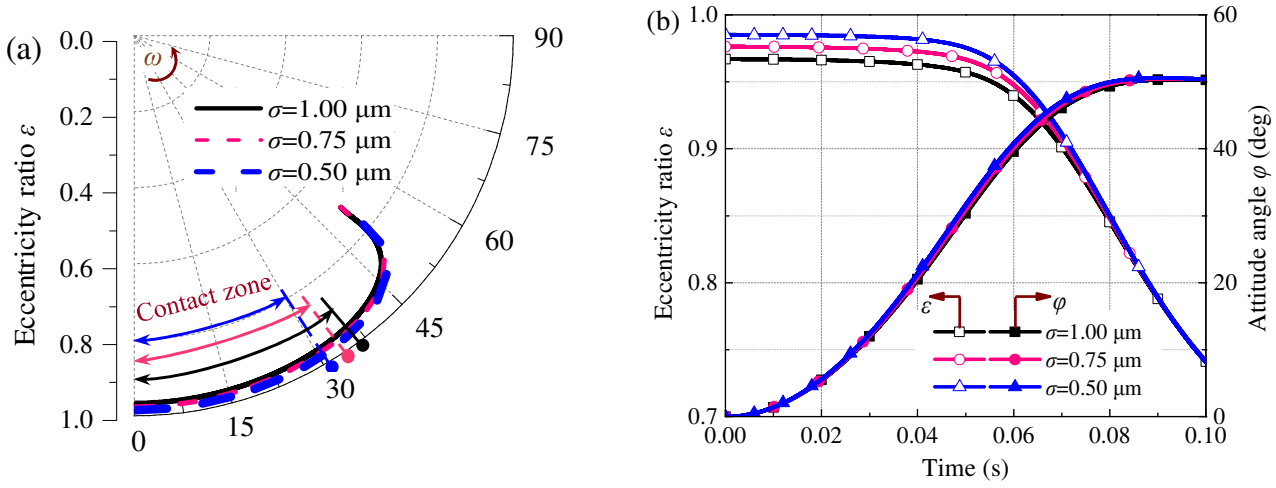

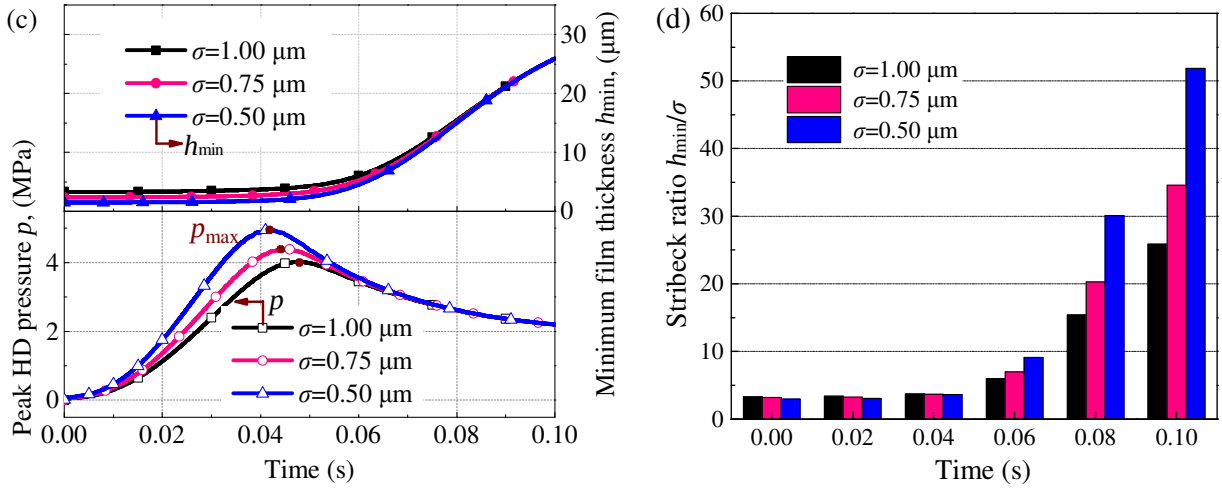

Fig. 6 The variations of transient characteristics of hydrodynamic cylindrical bearing in different standard deviation of asperity heights σ during startup, (a) journal center locus in clearance circle, (b) eccentricity ratio and attitude angle, (c) peak hydrodynamic (HD) pressure and minimum average film thickness, and (d) Stribeck ratio of h_{min}/σ

Fig. 7 depicts the distributions of hydrodynamic pressure and contact pressure in the plane of z=0 of the bearing in different standard deviation of asperity heights σ. We observe that at the initial time t=0 s, high peak contact pressure is caused by low σ. The maximum contact pressure reaches 14 MPa with σ=0.5 μm (Fig. 7 (a)). At the time of t=t_{pmax} (Fig. 6 (c)), the locations of both the maximum contact pressure (Fig. 7 (b)) and the maximum HD pressure (Fig. 7 (c)) moves forward at a small σ. At t=0.1 s, σ has a very slight effect on the HD pressure (Fig. 7 (d)).

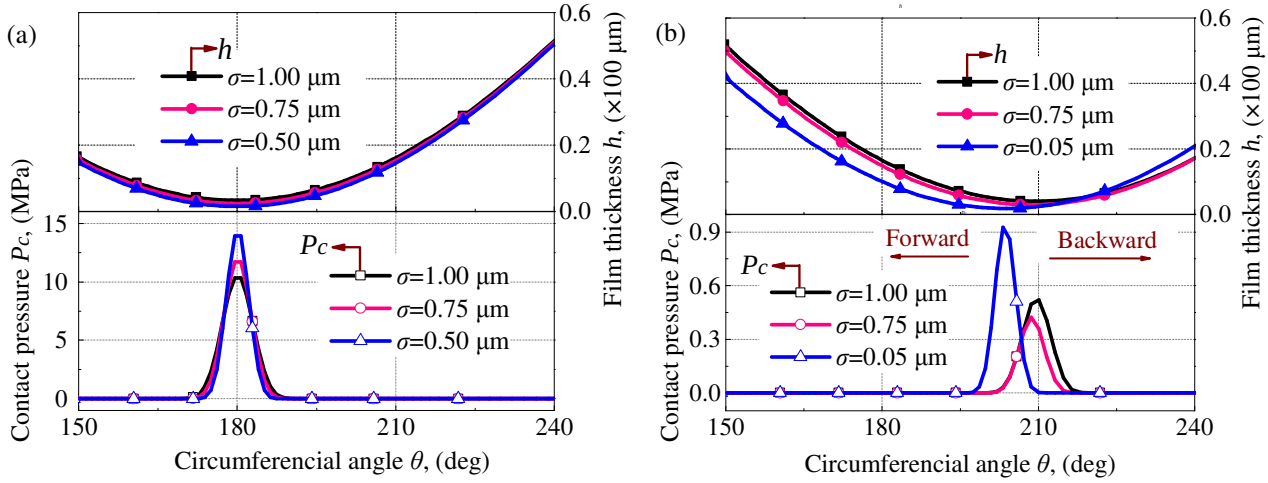

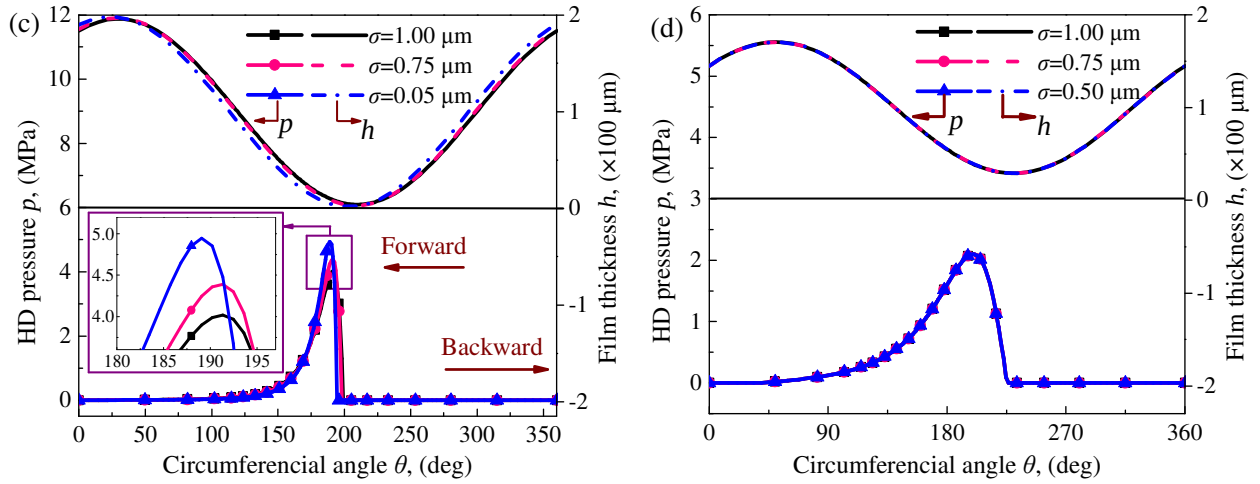

Fig. 7 The distributions of hydrodynamic (HD) pressure p, contact pressure P_c and film thickness h in the plane of z=0 in different standard deviation of asperity heights σ during startup, (a) contact pressure distribution at the initial time t=0 s, (b) contact pressure distribution at the moment the transient HD pressure peaks, i.e., $t=t_{pmax}$, (c) HD pressure distribution at the moment the transient HD pressure peaks, i.e., $t=t_{pmax}$, and (d) HD pressure distribution at t=0.1 s.

3.4 Effects of surface pattern

The surface pattern parameters are 1/6, 1 and 6 in transverse, isotropic and longitudinal orientations, respectively, as shown in Table 1. σ is set to be 1 μm. The rotational speed is set to rise up to 1000 rpm in 0.1 second. Other parameters are listed in Table 3.

Fig. 8 shows the influences of surface pattern on the transient characteristics of hydrodynamic cylindrical bearings during startup. It is obvious that the surface pattern has slight effects on both the movement and the hydrodynamic forces of the bearing during startup. Comparing to the transverse and isotropic surface patterns, the longitudinal surface pattern generates a slight increase in the eccentricity ratio (Fig. 8 (b)) but a slight decrease in the hydrodynamic bearing force (Fig. 8 (c)). Also, for longitudinal surface pattern, the minimum average film thickness is the smallest, while the peak hydrodynamic pressure is the lowest (Fig. 8 (d)). This means that the surface pattern in longitudinal orientation can decrease the carrying capacity slightly, which agrees with the conclusion of Dobrica et al. [14]. This is due to the micro-hydrodynamic effect generated by the micro-textures of surface roughness.

In general, under the present applied load, the influence of surface pattern on the transient characteristics of the bearing during startup is slight enough to be ignored. The reason is that the initial Stribeck ratio of the rough surfaces under the present applied load is about 3.3. At such a large Stribeck ratio, the effects of the factors Φ_θ , Φ_z and Φ_s) in Eq. (2a) can be neglected. However, if a heavy load is applied, the minimum film thickness is small, generating a low Stribeck ratio. The effects of the surface pattern will be more obvious [8].

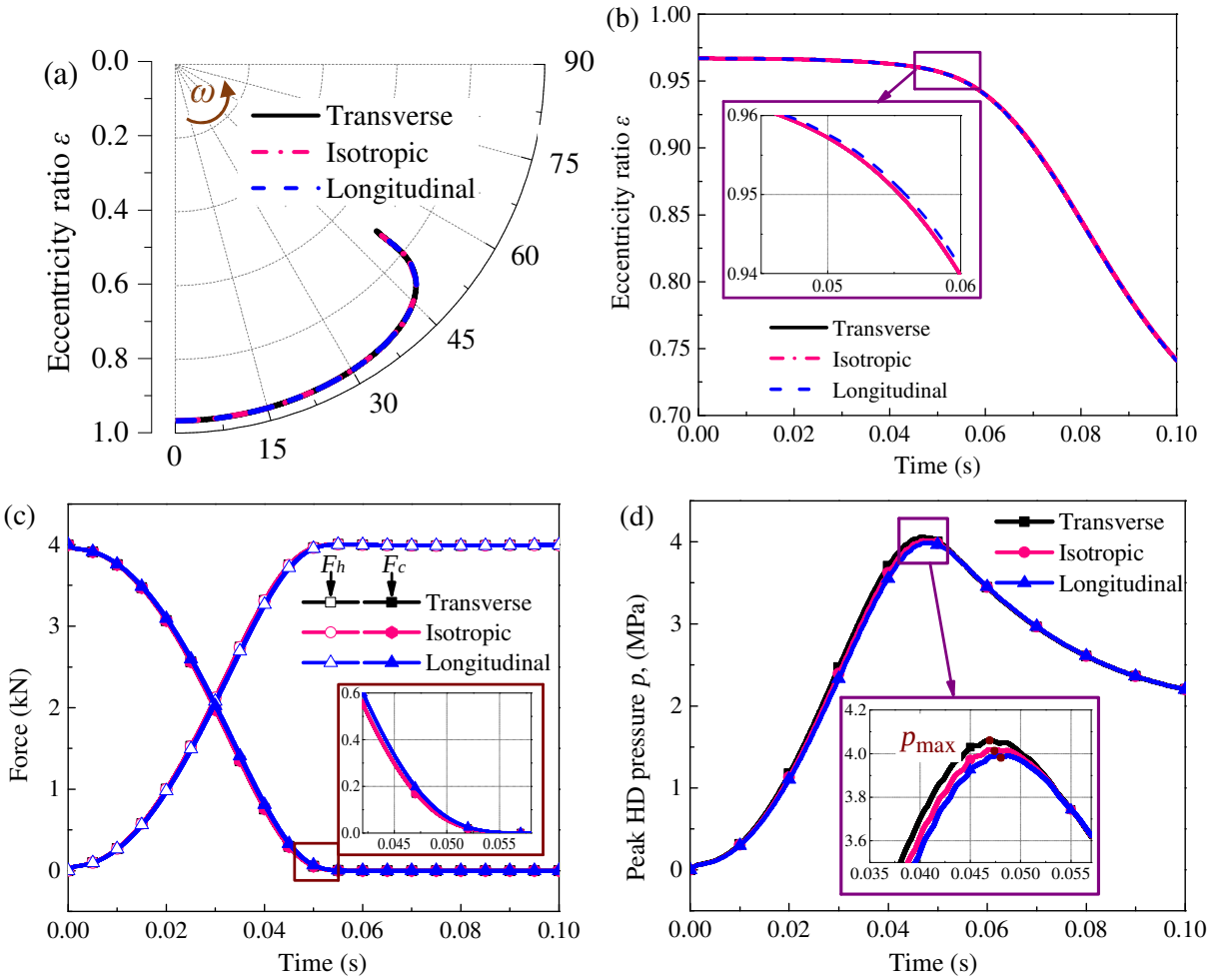

Fig. 8 The variations of transient characteristics of the hydrodynamic bearing in different surface patterns during startup, (a) journal center locus in clearance circle, (b) eccentricity ratio ε, (c) the hydrodynamic force F_h and contact force F_c, and (d) the transient peak hydrodynamic (HD) pressure p

Fig. 9 shows the distributions of contact pressure and hydrodynamic pressure in the plane of z=0 of the hydrodynamic cylindrical bearing in different surface patterns during startup. We observe that at the initial time t=0, the surface pattern has no influence on the contact pressure distribution and the average film thickness (in Fig. 9 (a)). At the moment of t=t_{pmax} when the hydrodynamic (HD) pressure reaches the maximum, the longitudinal roughness causes slight decrease in both maximum contact pressure and maximum HD pressure. The locations of both the maximum contact pressure and the maximum HD pressure move backward for the longitudinal surface pattern. (Fig. 9 (b) and (c)). In hydrodynamic lubrication (t=0.1 s), the influences of the surface pattern disappear in Fig. 9 (d).

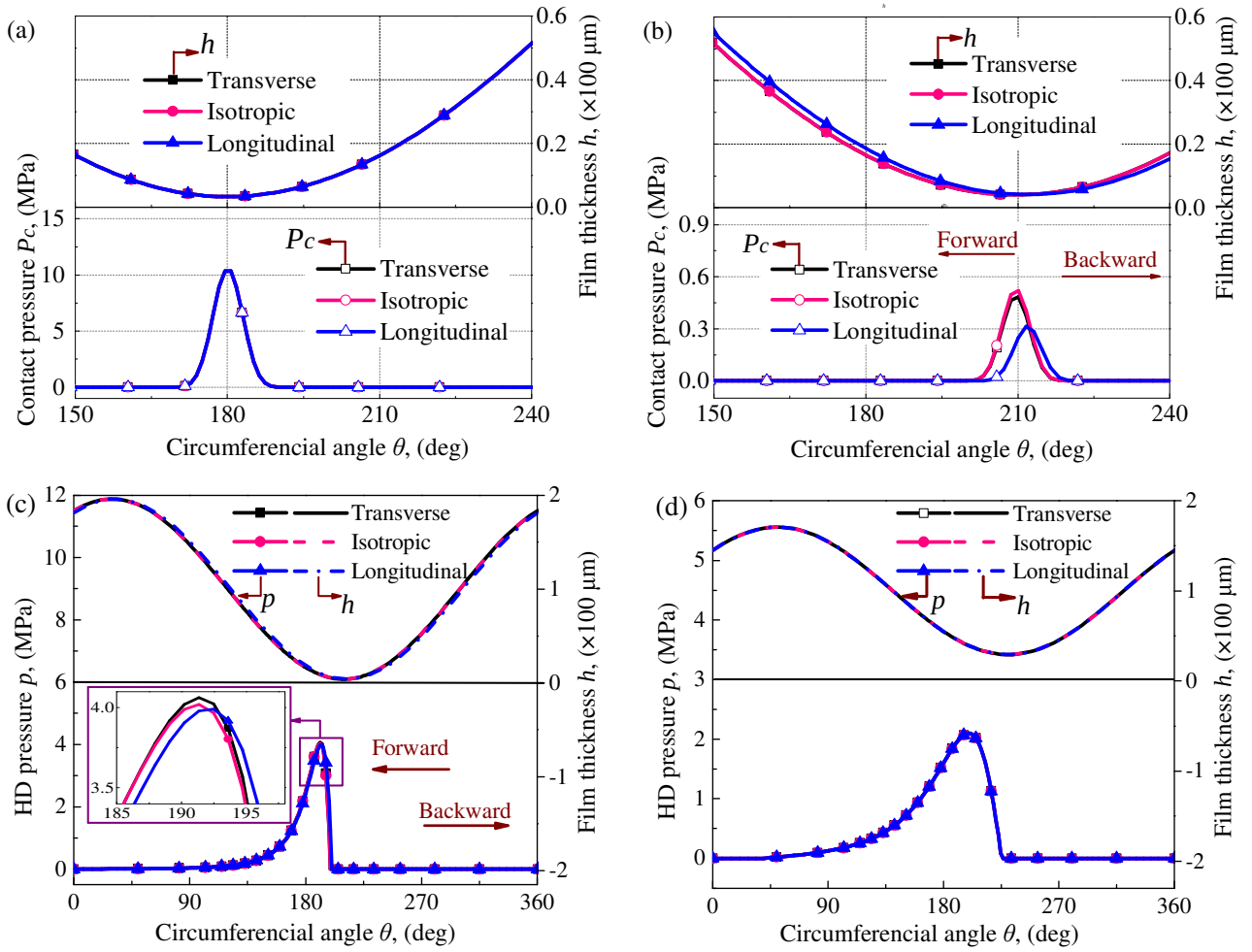

Fig. 9 The distributions of hydrodynamic (HD) pressure, contact pressure and average film thickness in the plane of z=0 in different surface patterns during startup, (a) contact pressure distribution at t=0 s, (b) HD pressure distribution at the moment when the transient HD pressure peaks, i.e., at t=t_{pmax}, (c) contact pressure distribution at the moment when the transient HD pressure peaks, i.e., at t=t_{pmax} and (d) HD pressure distribution at t=0.1 s.

4 Conclusions

The effects of surface roughness on the transient characteristics of hydrodynamic cylindrical bearings during startup are studied. From the results we concluded that:

1. During startup of the hydrodynamic cylindrical bearing, the minimum average film thickness keeps increasing. The peak hydrodynamic pressure first increases and then decreases, reaching a maximum value before the shaft separates with the bearing surface. The hydrodynamic active pressure zone increases. The contact pressure decreases, while the contact zone is not changed during contact time.

2. For the hydrodynamic cylindrical bearing during the initial period of startup, a small standard deviation of asperity height σ causes a high hydrodynamic pressure, a short contact time, a small sliding contact zone, and a small lift-off speed. However, the maximum hydrodynamic pressure increases with a decrease in σ.

3. The surface pattern has a slight but important effect on the transient behavior during contact time. The longitudinal surface pattern can slightly reduce the hydrodynamic bearing force, and increase both the contact time and the lift-off speed. Also, the longitudinal surface pattern generates a small maximum hydrodynamic pressure with a small minimum average film thickness.

Acknowledgment

The authors want to acknowledge the financial support from the National Natural Science Foundation of China (No. U1637206, No.51475452) and the Foundation for Innovative Research Groups of the National Natural Science Foundation of China (No.51521003).

5 References

[1] Hu Y, Zhu D. A full numerical solution to the mixed lubrication in point contacts. J Tribol 2000; 122(1): 1-9.

[2] Gertzos KP, Nikolakopoulos PG, Chasalevris AC, et al. Wear identification in rotor-bearing systems by measurements of dynamic bearing characteristics, Comput Struct 2011; 89(1): 55–66.

[3] Rao A, Mohanram PV. A study of mixed lubrication parameters of journal bearings. Wear 1993; 160(1): 111-118.

[4] Dufrane KF, Kannel JW. Thermally induced seizures of journal bearings. J Tribol 1989; vol. 111(2): 288-292.

[5] Wang Y, Zhang C, Wang Q, Lin C. A mixed-TEHD analysis and experiment of journal bearings under severe operating conditions. Tribol Int 2002; 35 (6): 395-407.

[6] Christensen H, Tonder K. The hydrodynamic lubrication of rough journal bearings. J of Lubrication Tech 1973; 95(2), 166-172.

[7] Patir N, Cheng HS. An average flow model for determining effects of three-dimensional roughness on partial hydrodynamic lubrication. J of Lubrication Tech 1978; 100(1): 12-17.

[8] Patir N, Cheng HS. Application of average flow model to lubrication between rough sliding surfaces. J of Lubrication Tech 1979, 101(2): 220-229.

[9] Wang Y, Wang Q, Lin C, et al. Development of a set of Stribeck curves for conformal contacts of rough surfaces. Tribol Trans 2006; 49(4): 526-535.

[10] Wang Q, Shi F, Lee S. A mixed-TEHD model for journal-bearing conformal contact—part II: contact, film thickness, and performance analyses. J Tribol 1998; 120 (2): 206-213.

[11] Shi F, Wang Q. A mixed-TEHD model for journal-bearing conformal contacts—part I: model formulation and approximation of heat transfer considering asperity contact. J Tribol 1998; 120(2): 198-205.

[12] Sander DE, Allmaier H, Priebsch HH, et al. Simulation of journal bearing friction in severe mixed lubrication–Validation and effect of surface smoothing due to running-in. Tribol Int 2016; 96: 173-183.

[13] Dobrica MB, Fillon M, Maspeyrot P. Mixed elastohydrodynamic lubrication in a partial journal bearing—comparison between deterministic and stochastic models. J Tribol 2006; 128 (4): 778-788.

[14] Dobrica MB, Fillon M, Maspeyrot P. Influence of mixed-lubrication and rough elastic-plastic contact on the performance of small fluid film bearings. Tribol Trans 2008; 51 (6): 699-717.

[15] Monmousseau P, Fillon M. Transient thermoelastohydrodynamic analysis for safe operating conditions of a tilting-pad journal bearing during start-up. Tribol Int 2000; 33 (3-4): 225-231.

[16] Pajączkowski P, Schubert A, Wasilczuk M, Wodtke M. Simulation of large thrust-bearing performance at transient states, warm and cold start-up. Proc IMechE Part J: J Engineering Tribology 2014; 228(1): 96–103.

[17] Cui S, Gu L, Wang L, et al. Numerical analysis on the dynamic contact behavior of hydrodynamic journal bearings during start-up. Tribol Int 2018; 121: 260-268.

[18] Mokhtar MOA, Hozarth RB, Davies PB. Wear characteristics of plain hydrodynamic journal bearings during repeated starting and stopping. ASLE Trans 1977; 20(3): 191-194.

[19] Mokhtar MOA, Howarth RB, Davies PB. The behavior of plain hydrodynamic journal bearings during starting and stopping. ASLE Trans 1977; 20(3): 183-190.

[20] Bouyer J, Fillon M. Experimental measurement of the friction torque on hydrodynamic plain journal bearings

during start-up. Tribol Int 2011; 44(7-8): 772-781.

[21] Sugimura J, Watanabe T, Yamamoto Y. Effects of surface roughness pattern on the running-in process of rolling/sliding contacts. In Tribology Series Elsevier 1994 ; 27: 125-137.

[22] Krupka I, Svoboda P, Hartl M. Effect of surface topography on mixed lubrication film formation during start up under rolling/sliding conditions. Tribol Int 2010; 43(5-6): 1035-1042.

[23] Pei S, Xu H, Shi F. A deterministic multiscale computation method for rough surface lubrication. Tribol Int 2016; 94: 502-508.

[24] Hu Y, Zhu D. A full numerical solution to the mixed lubrication in point contacts. J Tribol 2000; 122(1): 1-9.

[25] Zhang C, Jiang X, Wang L, et al. Effect of surface roughness on the start-stop behavior of air lubricated thrust micro-bearings. Tribol Int 2018; 119: 436-442.

[26] Wang XL, Zhu KQ. Numerical analysis of journal bearings lubricated with micropolar fluids including thermal and cavitating effects. Tribol Int 2006; 39(3): 227-237.

[27] Wu C, Zheng L. An average Reynolds equation for partial film lubrication with a contact factor. J tribol 1989; 111(1): 188-191.

[28] Greenwood J A, Williamson JP. Contact of nominally flat surfaces. In Proc R Soc Lond. A The Royal Society 1966; 295(1442): 300-319.

[29] Varney P, Green I. Rough Surface Contact of Curved Conformal Surfaces: An Application to Rotor–Stator Rub. J Tribol 2016; 138(4): 041401.

Nomenclature

C	radius clearance, $C=R-r$
d	general surface distance
D_{sum}	surface density of the asperity
e	eccentricity of the shaft in the bearing
E	elasticity modulus
E'	equivalent elasticity modulus, $1/E' = \left(1-\nu_1^2\right)/E_1 + \left(1-\nu_2^2\right)/E_2$
F_h, F_c	hydrodynamic bearing force and asperity contact force, respectively
h	average film thickness
H'	Stribeck ratio, $H' = h/\sigma$
H	nondimentional average film thickness, $H=h/C$
m	mass of the rotor
N_j	shape function, j = 1, 2, 3
p	hydrodynamic pressure
$\overline{P}$	individual asperity contact force
P	nondimentional hydrodynamic pressure, $P = p/p_a$, $p_a = 2\mu\omega/\psi^2$
P_j	nondimentional hydrodynamic pressure at each node, j = 1, 2, 3
P_c	contact pressure
R_p	radius of the asperity
R	bearing radius
r	shaft radius
t_c	contact time
u	velocity of the shaft surface

U	nondimentional velocity of the shaft surface, $U=u/(r\omega)$
v	Poisson's ratio
W	applied load
x, y, z	Cartesian coordinate
$\overline{z}$	standard separation of two surfaces
ε	eccentricity ratio, $\varepsilon=e/C$
φ	attitude angle
θ, λ	angular and axial coordinate, $\lambda= z/B$
ψ	relative clearance, $\psi =C/r$
σ	standard deviation of asperity height, R_q
μ	dynamic viscosity of the lubricant
ω	rotational speed of the shaft
ϖ	inference of asperities, $\varpi=\overline{z}-d$
δP	pressure change between consecutive iterations
γ	surface pattern parameter
ξ, η	nondimentional coordinates of the element, $-1\leq \xi, \eta \leq 1$
$f(\overline{z})$	density function of Gaussian distribution of the asperity height
Φ_θ, Φ_z	pressure flow factors in circumferential and axial directions, respectively
Φ_s, Φ_c	shear flow factor and contact factor, respectively
∇	gradient operator
$\mathbf{I}_{Gauss}$	Gaussian integration

Highlights

1. The problem of cylindrical journal bearing operating under transient regime is solved by a mixed lubrication model considering asperity contacts and hydrodynamic fluid flow.
2. The transient characteristics of hydrodynamic cylindrical bearings from mixed lubrication to hydrodynamic lubrication are presented.
3. The effects of standard deviation of asperity height and the rough surface pattern on the transient behavior during startup are analyzed.